Monitoring the excavation damaged zone by three dimensional reconstruction of the electrical resistivity

N. Lesparre, Dominique Gibert, Florence Nicollin, Christophe Nussbaum, Andy Adler

▶ **To cite this version:**

N. Lesparre, Dominique Gibert, Florence Nicollin, Christophe Nussbaum, Andy Adler. Monitoring the excavation damaged zone by three dimensional reconstruction of the electrical resistivity. Geophysical Journal International, 2013, 195 (2), pp.972-984. 10.1093/gji/ggt282 . insu-00912987

HAL Id: insu-00912987
https://insu.hal.science/insu-00912987

Submitted on 6 Jul 2017

HAL is a multi-disciplinary open access archive for the deposit and dissemination of scientific research documents, whether they are published or not. The documents may come from teaching and research institutions in France or abroad, or from public or private research centers.

L'archive ouverte pluridisciplinaire **HAL**, est destinée au dépôt et à la diffusion de documents scientifiques de niveau recherche, publiés ou non, émanant des établissements d'enseignement et de recherche français ou étrangers, des laboratoires publics ou privés.

Geophysical Journal International

Geophys. J. Int. (2013) **195,** 972–984
Advance Access publication 2013 September 3

doi: 10.1093/gji/ggt282

Monitoring the excavation damaged zone by three-dimensional reconstruction of electrical resistivity

Nolwenn Lesparre,[1,2] Dominique Gibert,[2,3] Florence Nicollin,[3] Christophe Nussbaum[4] and Andy Adler[1]

[1]*Department of Systems and Computer Engineering, Carleton University, Ottawa, Ontario* K1S 5B6*, Canada. E-mail: lesparre@ipgp.fr*
[2]*Institut de Physique du Globe de Paris, Sorbonne Paris Cité, Univ Paris Diderot, UMR* 7154 *CNRS, Paris, France*
[3]*Géosciences Rennes (CNRS UMR* 6118*), Université Rennes* 1*, Bât.* 15 *Campus de Beaulieu, F-*35042 *Rennes cedex, France*
[4]*Swisstopo, Federal Office for Topography, Seftingenstrasse* 264*, CH-Wabern, Switzerland*

Accepted 2013 July 15. Received 2013 July 1; in original form 2012 May 29

SUMMARY

A damaged zone is formed during the excavation of underground galleries, altering the rock properties. From a perspective of nuclear waste storage in deep geological sites, there is a clear interest to monitor the rock properties in such zones. We constructed electrical resistivity tomograms as a function of time to monitor the damaged area in gallery 04 of the Mont Terri underground rock laboratory (Switzerland). Measurements were performed using electrode rings surrounding the gallery. The experience showed a heterogeneous distribution of damages around the gallery and their fast formation after the excavation. Two main areas were concerned by damage formation, located in regions where the bedding was tangential to the excavated gallery. Such regions represented an extension of about 2 m along the gallery walls and reached a depth of 1.5 m. Main damages were created during the next months following the excavation process. Slight variations were still observed 3 yr after the excavation that may be related to the gallery environmental condition fluctuation. The method applied here demonstrates the interest to monitor the whole region surrounding excavated galleries dedicated to host nuclear wastes.

Key words: Image processing; Tomography; Electrical properties; Geomechanics.

1 INTRODUCTION

Galleries of underground radioactive waste repositories are surrounded by an excavation damaged zone (EDZ) formed by the alteration of rock properties due to the stress perturbation produced by both the excavation process and the void of the galleries (Bossart *et al.* 2004). The EDZ has a thickness of about one gallery diameter (Bossart *et al.* 2004; Nussbaum *et al.* 2011) where the pore geometry is modified, pre-existing faults or cracks are reopened, and new ones are created. The EDZ then constitutes a privileged pathway where radionuclides may migrate from shafts and galleries to aquifers and eventually to the atmosphere. The EDZ is thus a particularly important issue in the safety evaluation procedure, and a great deal of work has been devoted to EDZ study (Alheid *et al.* 2002; Kruschwitz & Yaramanci 2004; Gibert *et al.* 2006; Marschall *et al.* 2006; Blümling *et al.* 2007; Nicollin *et al.* 2008; Le Gonidec *et al.* 2011; Schuster *et al.* 2011; Wassermann *et al.* 2011; Maineult *et al.* 2013).

Imaging and monitoring the EDZ is essential to evaluate its extend and degree of alteration. The EDZ formation strongly depends on initial and technical conditions—regional stress tensor, pre-existent fractures, geological facies, cross-section and arrangement of galleries, excavation process, wall structure—and its characterization cannot be done at a single experimental test site. Instead, to get an as complete view as possible, the EDZ must be studied at several places representative of orientation, rock facies, pre-existing condition, ... Also, detailed local auscultations may be mandatory due to particular conditions like junction of galleries, shafts and boreholes, particular geological feature. Light and reliable non-invasive imaging methods are complementary to reach these objectives and, among the geophysical techniques at our disposal, onsite electrical resistivity tomography (ERT) is particularly recommended for its great sensitivity to rock fracturing and its easy implementation.

The main objective of this study is to discuss ERT experiments performed in the Mont Terri underground rock laboratory (Switzerland) before and after the excavation of the gallery 04 (Fig. 1), and confront them to detailed geological and structural studies (geological mapping, boreholes, local injections of resin) performed in the same area (Marschall *et al.* 2006; Möri *et al.* 2010; Nussbaum *et al.* 2011). These ERT experiments constitute a unique data set covering a period of nearly 4 yr (2004 July–2008 April) during which

© The Authors 2013. Published by Oxford University Press on behalf of The Royal Astronomical Society.

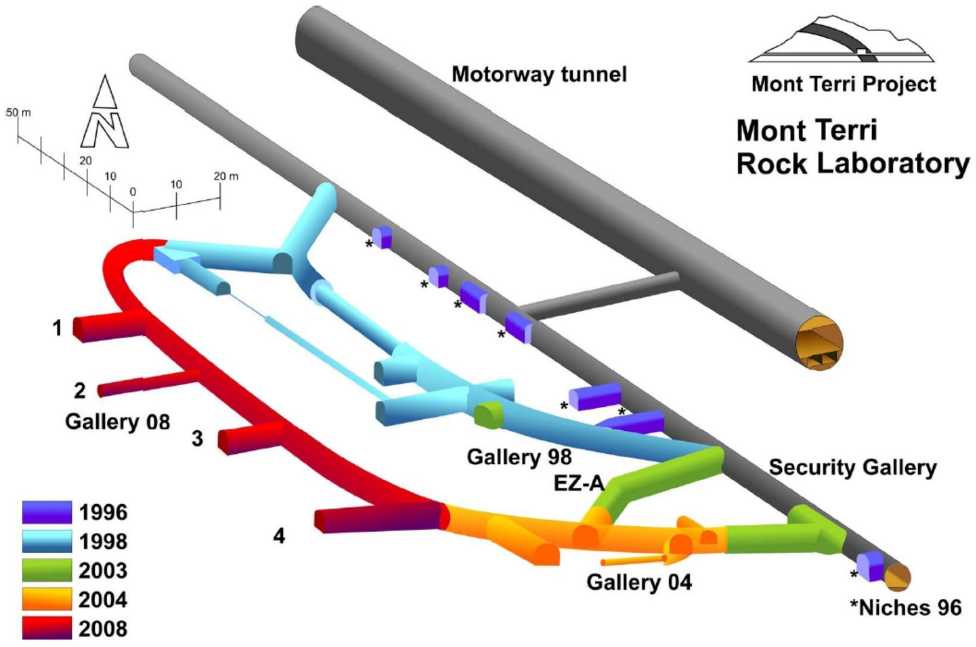

Figure 1. Mont Terri underground laboratory. Our experiment is located at the entrance of the gallery 04 at the intersection between the green and yellow regions.

repeated measurements were performed on fixed electrode arrays to follow the short- and mid-term evolution of the EDZ after the excavation of a large gallery.

The paper is organized as follows. Section 2 briefly reviews EDZ studies performed in the Mont Terri laboratory followed by a brief account of our present knowledge about EDZ formation and evolution. Section 3 gives details on the ERT experiments and presents the data set inverted in Section 4 where the resistivity tomograms are interpreted and discussed in regard of the knowledge on the EDZ formation gained from previous experiments. To focus on the results and on our understanding of the EDZ with ERT imaging, the technical issues concerning ERT 3-D inversion are given in Appendices. A conclusion recalls the main results and formulates some recommendations on the capabilities of ERT techniques to characterize the EDZ.

2 CONTEXT OF THE EXPERIMENT

2.1 Imaging the EDZ

In the Mont Terri underground rock laboratory, the EDZ has been extensively studied by *in situ* experiments performed in an Opalinus Clay formation. The Opalinus Clay, an argillaceous formation dated from the Aalenian (180 Myr) presents indeed excellent properties to host nuclear waste storage sites. In particular, this overconsolidated shale formation possesses a very low permeability with a hydraulic conductivity less than 10^{-12} m s^{-1}, so the transport of radionuclides is considerably reduced. And, if an EDZ is created by a gallery excavation, the Opalinus Clay has the property of self-sealing when interacting with infiltrated water, and its hydraulic conductivity dramatically decreases within a few years when in contact with wet air (Meier *et al.* 2000; Bossart *et al.* 2004; Blümling *et al.* 2007).

Structural observations showed that the EDZ properties mainly depend on the initial stress field, the nature of the embedding rock and the method of excavation (Bossart *et al.* 2004). In the Mont Terri Opalinus Clay, the EDZ was observed from the borehole scale to the gallery scale (Fig. 2) , highlighting its conspicuous relationships with the geology (facies, bedding) and with the pre-existing tectonic structures (Yong *et al.* 2010; Nussbaum *et al.* 2011; Wassermann *et al.* 2011; Thovert *et al.* 2011; Le Gonidec *et al.* 2012; Maineult *et al.* 2013). Two domains may be distinguished: a highly fractured inner shell and an outer shell extending several metres around the gallery. The inner shell about 1 m thick forms an interconnected fracture network connected to the excavated gallery, while in the outer shell, the fractures are unconnected or partially connected (Bossart *et al.* 2004; Nussbaum *et al.* 2011). Along boreholes, a study of the mechanical properties gave an estimate of the EDZ depth ranging from 0.6 to 2.2 m (Schuster *et al.* 2001; Alheid *et al.* 2002).

Seismic and acoustic experiments revealed a high heterogeneity of the EDZ and a strong anisotropy, presenting a factor of about 1.3, due to clay bedding (Schuster *et al.* 2001; Alheid *et al.* 2002; Nicollin *et al.* 2008; Le Gonidec *et al.* 2012). Because of both the soft nature of clay and the presence of cracks and fractures in the EDZ, the mechanical waves strongly attenuate, limiting the investigation depth of high-frequency seismic methods. With a larger investigation range and a lower resolution, electrical resistivity methods are able to provide information on the whole EDZ structure (Alheid *et al.* 2002; Kruschwitz & Yaramanci 2004; Gibert *et al.* 2006; Mayor *et al.* 2007; Thovert *et al.* 2011). The rock dehydration produced by air penetration in the connected fracture network highly increases the electrical resistivity of the damaged area, making the ERT a well-suited method to determine the bulk geometry of the EDZ and to monitor its evolution.

2.2 Mechanical processes inducing breakouts

The formation of the EDZ and the involved processes were studied by Marschall *et al.* (2006), from observations in a microtunnel drilled from the HG-A niche (Fig. 3). Breakouts as high as 15 cm, corresponding to cracks created or reopened during the excavation, are mainly observed in two opposite regions and involve two

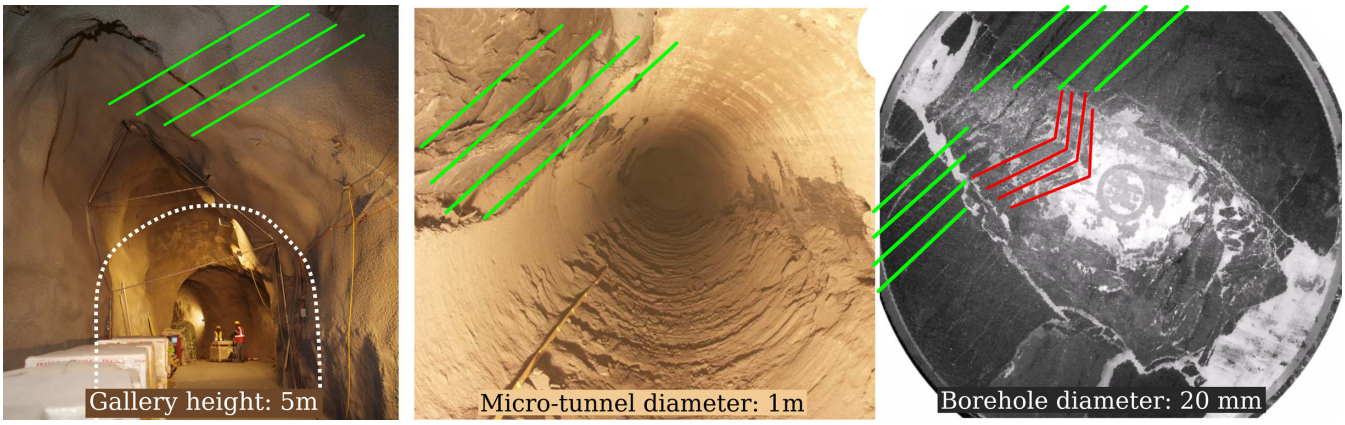

Figure 2. Influence of the bedding on buckling observed at different scales. From left to right: around the EZ-A niche of the Mont Terri laboratory (photo: Comet photoshopping, Zürich), around the HG-A microtunnel and around a borehole (photos: Mont Terri project, Swisstopo). The bedding is represented by the green lines.

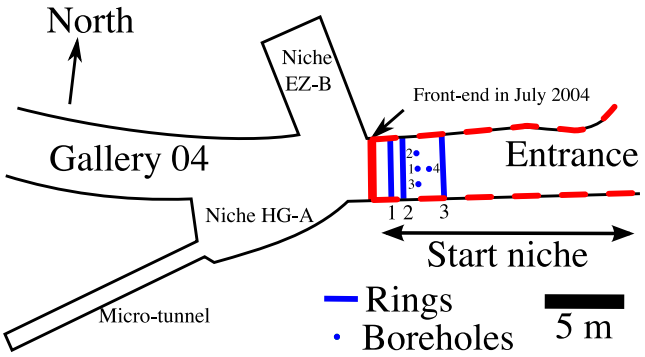

Figure 3. Top view of the gallery 04 entrance including the rings and boreholes location. The red line indicates the position of the gallery front-end in 2004 July and the start niche is represented by the red dashed line. Boreholes BEZ-G1, G2 and G4 are vertical downwards, while BEZ-G3 is oblique upwards (see Fig. 6).

coexistent processes (Fig. 4). Where bedding is tangential to the tunnel wall, slab-like breakouts are created by buckling, eventually in connection to tectonic fractures subparallel to the bedding. Breakouts are less significant in the region located near the floor where debris remained in place with a gravity effect less important. The second mechanism creating failures and wedge-like breakouts is mainly controlled by stress anisotropy. Thus, the emergence of the EDZ is triggered by the bedding that acts as sliding planes further reducing the mechanical stability. Onion-like extension joints then appear with an orientation parallel to the tunnel walls.

2.3 Seasonal variations of the gallery environment

Seasonal variations of environmental conditions—that is, temperature and humidity—in the galleries may be partly responsible of observed variations of electrical resistivity. Temperature seasonal variations in the Mont Terri underground laboratory are greatly attenuated and temperature varies only from 8°C in winter to 13°C in summer (Möri *et al.* 2010). Studies performed with near-surface sediments show that even such moderate temperature variations may significantly change the electrical resistivity (Hayley *et al.* 2007). Owing to these results, the temperature variations observed in the Mont Terri galleries may produce a decrease of about 5–10 per cent of the electrical resistivity in summer. Correcting this effect (Hayley *et al.* 2010) in the data analysed in this study is presently impossible because of the lack of data available to constrain models.

Seasonal variations of relative humidity may also produce changes of electrical resistivity through opening and closing of fractures as observed in the EZ-B niche (Möri *et al.* 2010). A clear anticorrelation is observed between relative humidity level and fracture aperture. Fractures open in winter when the gallery is dry and they partly close under moist summer conditions (Fig. 5). In the presence of high levels of humidity, negative variations of the pressure induce swelling of the argillaceous formation. However, during dry climate, cracks reopen as an unsaturated area develops from high suction pressures present on the tunnel walls (Möri *et al.* 2010). Such cyclic behaviour may enhance the strength of the excavation damage (Marschall *et al.* 2006). The knowledge of such mechanisms in the EDZ formation and cyclic fluctuations further motivates the need to develop monitoring methods and supply clues to understand images obtained from geophysical measurements. Electrical resistivity is expected to decrease in summer when the closure of fractures reduces the quantity of voids present in the bulk clay and reestablish electrical contact between crack sides. Consequently, both the temperature and the humidity increases observed in summer may coherently provoke a decrease of electrical resistivity in the first tens of centimetres of the EDZ.

3 FIELD EXPERIMENTS

The electrical resistivity measurements were made at the end of the 20 m long and 5 m wide gallery 04 start niche excavated in 2004 March. Three rings labelled 1, 2, 3 and counting 32 equispaced electrodes were placed, respectively, at 1, 1.5 and 4 m from the end-face of the niche (Fig. 3, 6). The electrodes are stainless steel rods with a diameter of 8 mm embedded in the clay to a depth of 5 cm. The distance between nearby electrodes is 0.55 m.

Measurements were acquired with a circular Wenner electrode arrangement (Gibert *et al.* 2006), and less-standard protocols were also used to increase the amount of information on the medium resistivity. The first set of measurements was performed in 2004 July prior to the excavation of the gallery 04 (GA04), and the next measurements were done in 2004 September, 2 weeks after the restart of the excavation, when the end-face of GA04 was at a distance of 20 m. Measurements took place in 2004 December and 2005 January, prior and after the excavation of the EZ-B and HG-A niches,

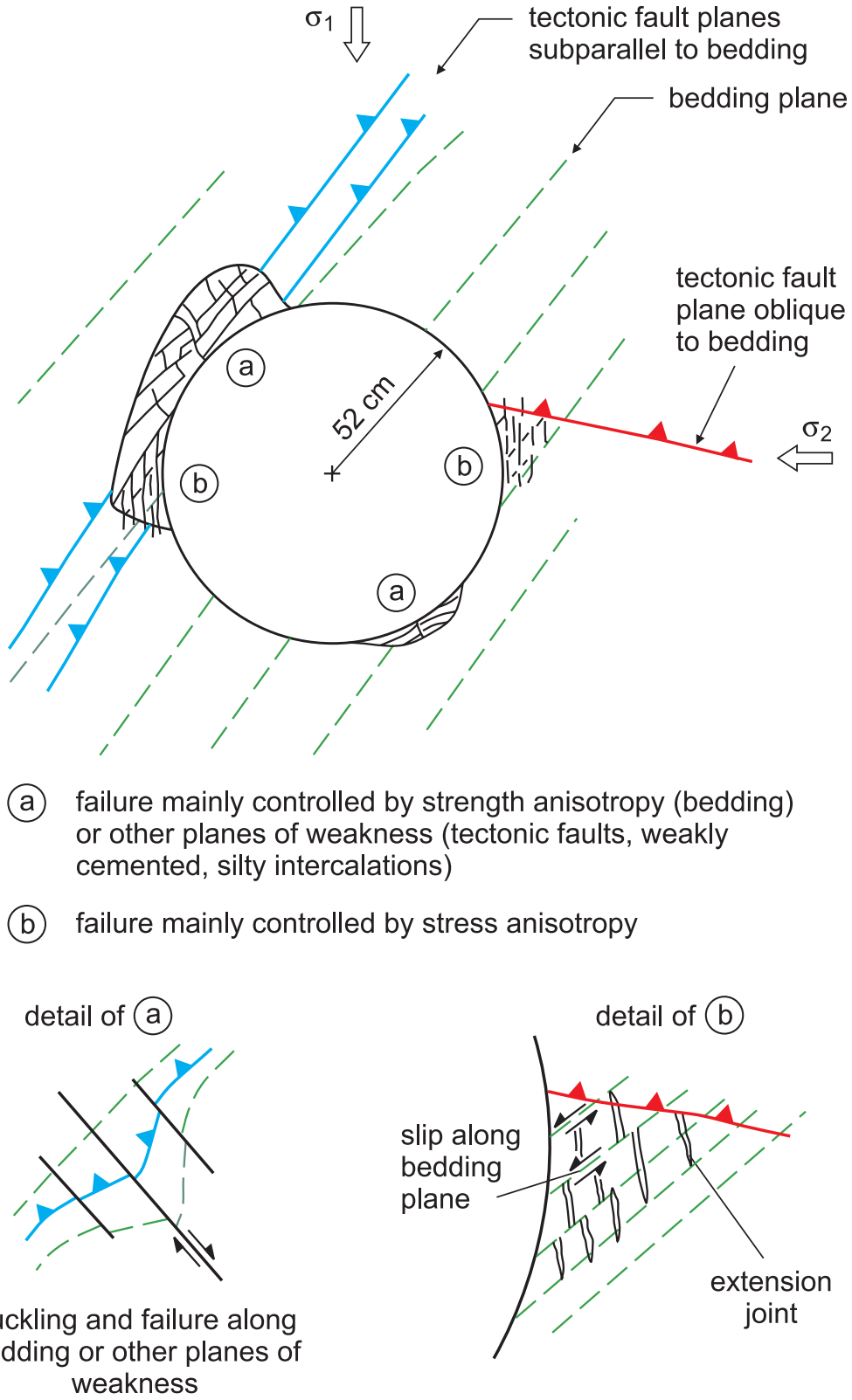

Figure 4. Mechanisms of breakouts formation after the microtunnel excavation due to strength and stress anisotropy, from Marschall *et al.* (2006).

respectively, located in the north and south side walls of GA04 at a distance of about 1 m from ring 1 (Fig. 3). Other measurements were made in 2005 March, 2006 April, 2007 September and 2008 April to monitor long timescale variations of the rock electrical resistivity around the gallery. Four boreholes were also drilled in the last part of the experiment and equipped with electrodes.

The eight data sets analysed in this study were acquired by using the same procedure: an electrical current of 100 mA is injected in

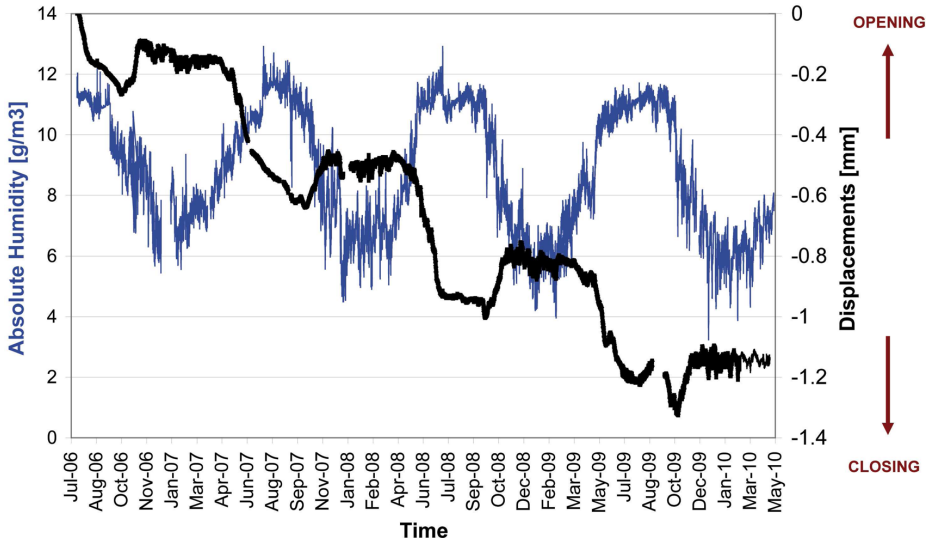

Figure 5. Variations of the relative humidity and fracture displacement (opening and closing) measured in the niche EZ-B (Möri *et al.* 2010).

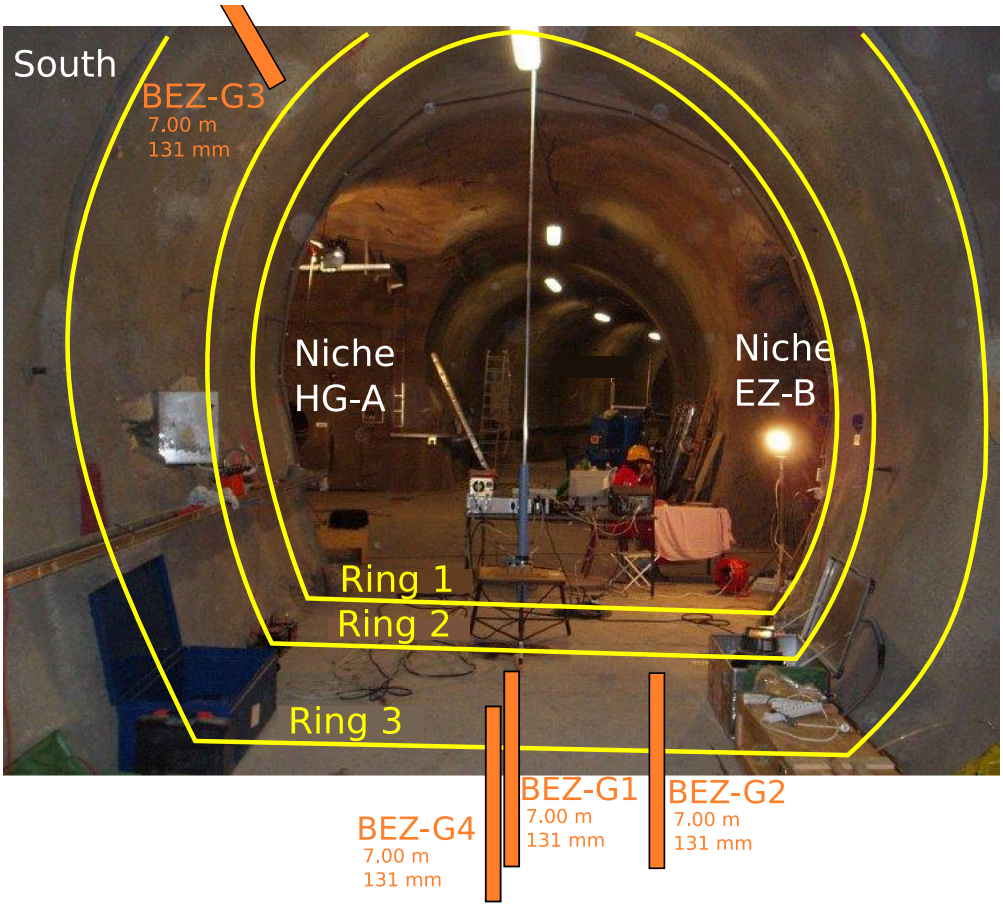

Figure 6. Picture at the entrance of gallery 04 and scheme of the electrodes rings and boreholes equipped for electrical measurements.

the medium between electrodes A and B, and the voltage measured between electrodes M and N is converted into apparent resistivity by using a forward model of the gallery with a homogeneous conductivity. This renormalization compensates the huge discrepancy of one or two order of magnitude between voltages measured on nearby electrodes and those measured on distant electrodes. Apparent resistivity gives the same weight to all data.

4 RESISTIVITY TOMOGRAMS AND INTERPRETATIONS

4.1 Electrical resistivity tomograms

The inversion of the apparent resistivity data involves a 3-D finite elements forward modelling that reproduces the geometry of

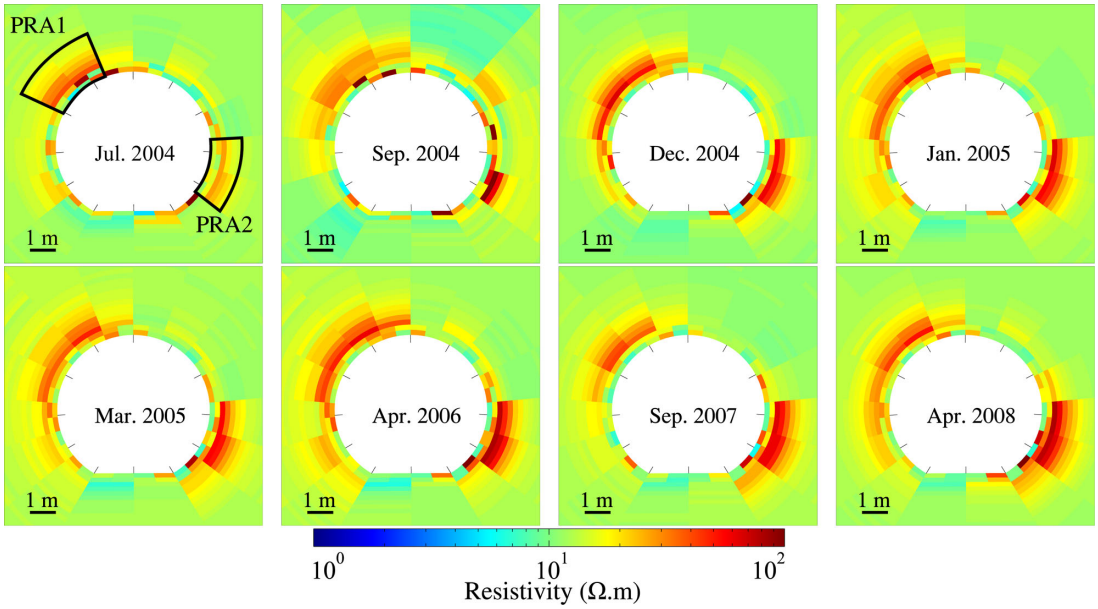

Figure 7. Evolution of the average resistivity with time during the process of gallery 04 excavation from 2004 July to 2008 April. North is on the right side.

the gallery and a fine meshing is used in the vicinity of the rings of electrodes. The limited amount of data available would make a full 3-D inversion of the conductivity distribution hugely underdetermined. Consequently, we reconstruct three 2-D conductivity structures, in the planes of the electrodes rings, interpolated along the axis of the gallery segment as described in the Appendix A. The resistivity tomograms present the electrical resistivity averaged over the three rings for all measurement periods (Fig. 7). The data are inverted through an iterative linearized procedure detailed in Appendix A.

4.2 Global resistivity structure

The resistivity tomograms possess a common global structure with two resistive anomalies located on opposite sides of the gallery (Fig. 7). A first persistent resistive anomaly (PRA1) is located in the 9hr–12hr sector and another one (PRA2) in the 3hr–5hr sector (see Fig. 8 for clock-like positioning). These two resistive structures have a size of about 2 m along the circumference of the gallery and a depth of 1.5 m.

The pattern depicted by the resistivity tomograms is identical to the breakout structure observed in the microtunnel (Fig. 4) and coherent with the high-resolution geological mapping performed during GA04 excavation (Gibert *et al.* 2006, Fig. 9). In particular, the bedding and the tectonic fault planes near the rings present a similar orientation with respect to the excavations in GA04 start niche and in the microtunnel (Fig. 4). The two resistive anomalies PRA1 and PRA2 may safely be attributed to the presence of highly damaged clay. The resistivity values in these areas are comprised between 20 and 100 Ω m in full accordance with Kruschwitz & Yaramanci (2004) who found resistivities between 16 and 60 Ω m in the damaged zones.

The resistivity at depths >2 m appears almost homogeneous with moderate variations from one period to another. The average resistivity is 11.8 Ω m for a standard deviation of 1.6 Ω m. This value falls near the constant background resistivity of 11 Ω m fixed at depths larger than 6 m in the forward modelling and estimated

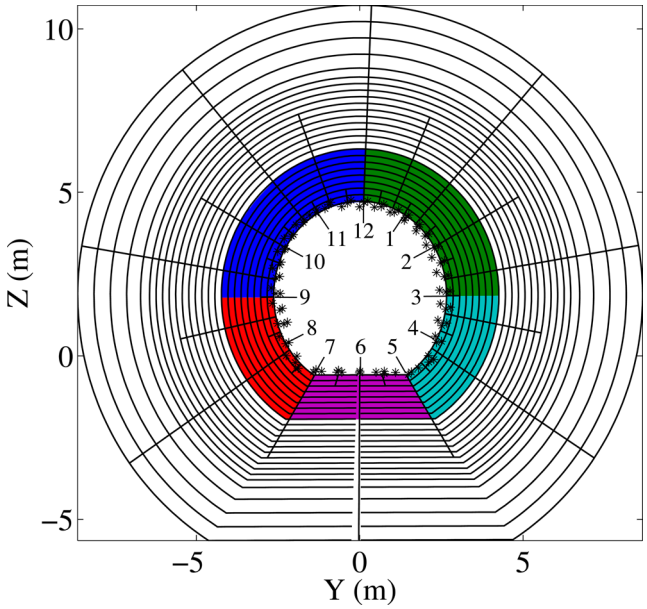

Figure 8. Parametrization of the inverse problem. From the gallery wall, concentric layers are created and divided into sectors which size increases as they are located far from the gallery walls. The stars represent the electrodes positions and the numbers correspond to the position of the clock hours used later for the images description and interpretation. Coloured sectors correspond to curves (Fig. 11).

from boreholes measurements. Such resistivity values are in full agreement with those (8 and 16 Ω m) obtained by Kruschwitz & Yaramanci (2004) for the undisturbed Mont Terri Opalinus Clay. Consequently, the resistivity inverted for depth beyond 2 m does not significantly differ from resistivity of undisturbed clay. A low persistent resistivity value of about 8 Ω m is found in the floor zone (5hr–7hr) and probably corresponds to a region of fully saturated rock not solicited by EDZ formation (Fig. 7; Kruschwitz & Yaramanci 2004). The fractures observed on the cores correspond

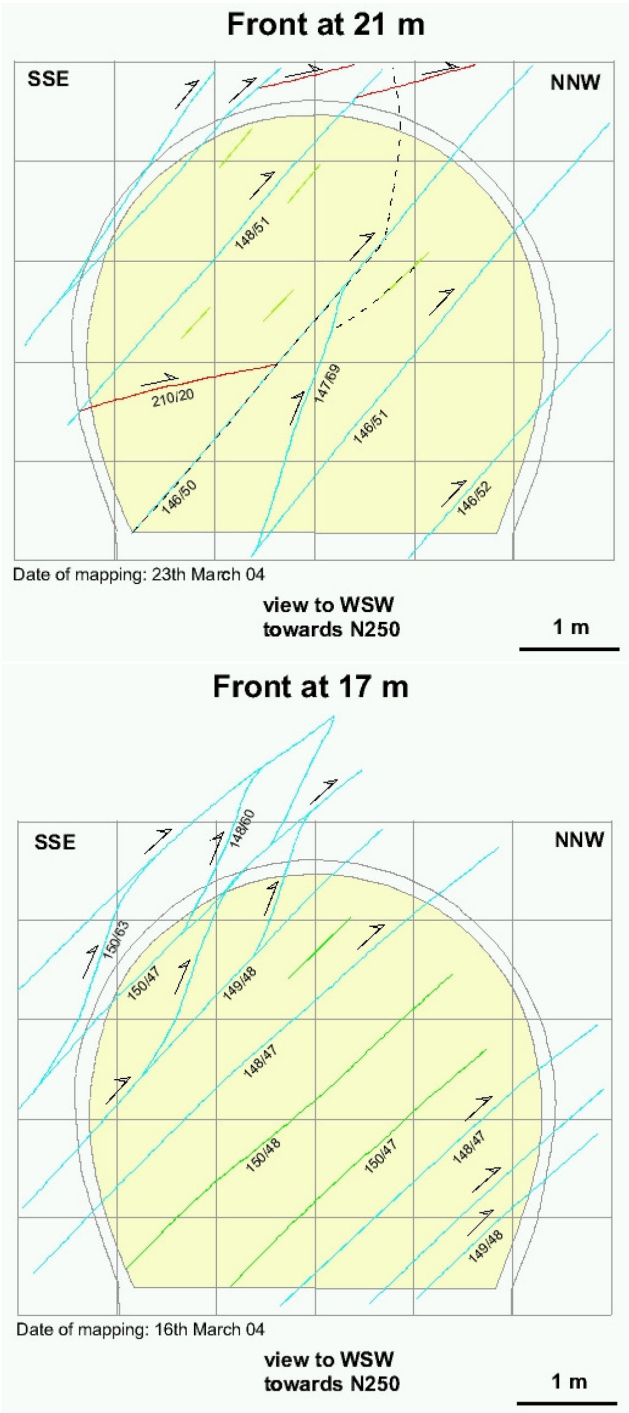

Figure 9. Orientation of main faults and bedding at the level of the end-face (top panel) and ring 3 (bottom panel), from Gibert *et al.* (2006).

indeed mainly to pre-existing faults in the plane of the bedding and rarely to EDZ. Only two EDZ unloading joints are distinguished on the cores extracted from the three boreholes excavated on the ground (Fig. 6).

4.3 Resistivity variability along the gallery

We now address the validity of the reconstruction procedure used for the tomograms discussed in the previous section. For this purpose, we present the three individuals tomograms corresponding to

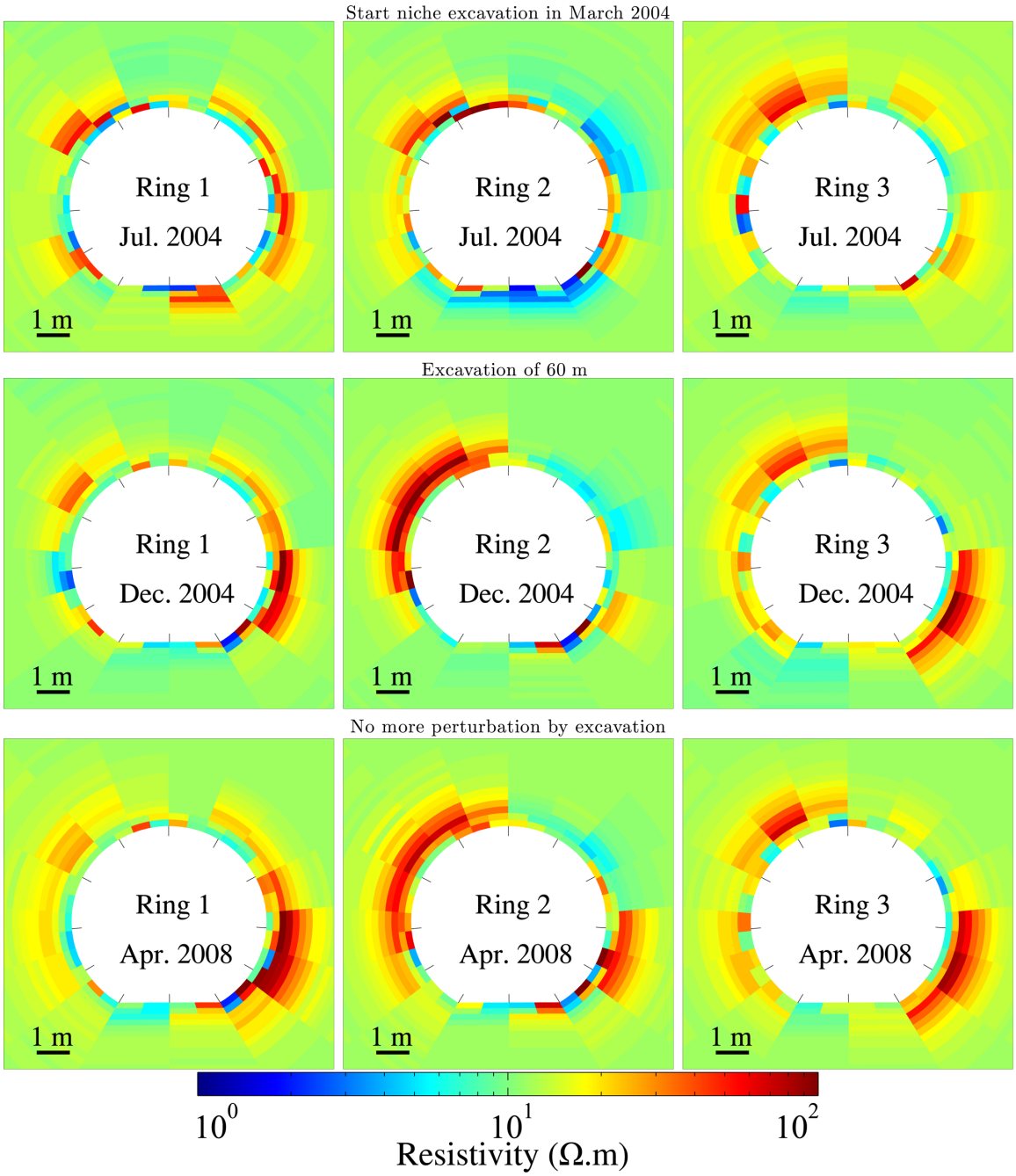

Figure 10. Reconstructed resistivities around rings 1, 2 and 3 during the process of the gallery GA04 excavation between 2004 July and 2008 April. North is on the right side.

the location of each ring of electrodes (Fig. 10). The forward modelling used in the inversions accounts for the geometrical changes produced by the excavation work: presence of end-face of GA04 near ring 1 in 2004 July, and appearance of the EZ-B and HG-A niches after 2004 December. The resistivity tomograms for the three rings are simultaneously inverted as explained in Appendix A.

We warn the reader that individual tomograms may be altered by noise due to the small amount of data used and of possible experimental conditions like missing electrodes. However, most differences observed in the tomograms from one ring to another appear correlated with features recognized during the geological mapping. For instance, the tomograms of 2004 July reveal the existence of a wider and deeper resistive zone in ring 3 at 10hr–12hr than observed in rings 1 and 2 (Fig. 10). This large resistive anomaly coincides with a high density of fractures at the level of ring 3 (bottom panel of Fig. 9) that necessitated bolting to secure the gallery's roof and is not present at rings 1 and 2 (top panel of Fig. 9).

An important increase of the resistive region located at 10hr–12hr is observed from 2004 July to December for ring 2 (Fig. 10). This event is clearly linked to the restart of the excavation work of GA04 and indicates an extension of the EDZ at this location along the gallery. The development of EDZ in this region agrees with onsite observations made at this period that report the appearance of important damage in the concrete wall in 2004

September and October that implied the reinforcement of the shotcrete layer.

Although corresponding to data sets acquired more than 3 yr after the end of the excavation work, the tomograms of 2008 April still display striking differences from one ring to another. So we note the persistence of the variability of the EDZ at plurimetric scale with respect to the main structures observed in the average tomograms (Fig. 7). The examples discussed in this section show that individual resistivity tomograms may be used to map the local variability of the damages caused by the excavation and which strongly depend on local conditions. Conversely, global tomograms (Fig. 7) are useful to smooth out small-scale features and reconstitute the main resistivity structure of a segment of gallery.

4.4 Electrical resistivity time variation

The data sets analysed in this paper cover a period of about 4 yr and provide information on the short- and medium-time variations of the electrical resistivity around the gallery. Short-time variations are visible in the selected individual tomograms of Fig. 10 in clear connexion with excavation progress like, for instance, the huge development of the 10hr–12hr resistive region of ring 2 between 2004 July and December.

To analyse time variations of resistivity, the evolution of the median resistivity in four angular sectors around rings 1 and 3 are represented (Fig. 11). The considered sectors cover 9hr–12hr, 12hr–3hr, 3hr–5hr and 5hr–7hr and go from the surface to a depth of 1.5 m. The curves for both rings show the same twofold structure with short-time variations of high amplitude occurring during the first 6 months after the restart of the excavation followed by a long period of nearly 3 yr during which the resistivity of each sector varies smoothly. This contrasting behaviour indicates that most perturbations due to the excavation occur within the following 6 months and afterwards a long-period evolution follows.

4.4.1 Short timescale

Regions located in sectors 12hr–3hr and 5hr–7hr have a low electrical resistivity $<15\ \Omega$ m (purple and green curves of Fig. 11) during the whole period and are moderately perturbed by the excavation process. A such observation agrees with the fact that these areas are located in regions less affected by breakouts formation (Fig. 4, Marschall *et al.* 2006). Conversely, the resistivity of the PRA1 and PRA2 sectors (blue curves of Fig. 11) shows more important variations during the first 6 months in agreement with the location of these regions where most breakouts are expected (Fig. 4).

These time variations appear complex and partly anticorrelated until the excavation of the niches. The decrease of resistivity observed during excavation in PRA2 for ring 1 is similar to the phenomenon reported by Kruschwitz & Yaramanci (2004) who invoked a close-up of microcracks due to stress release during the excavation followed by a reduction of the pore space and water content. Alternatively, the increase in resistivity might also reflect breakouts formation as observed by Marschall *et al.* (2006). The short-time variations of resistivity at individual rings are however quite

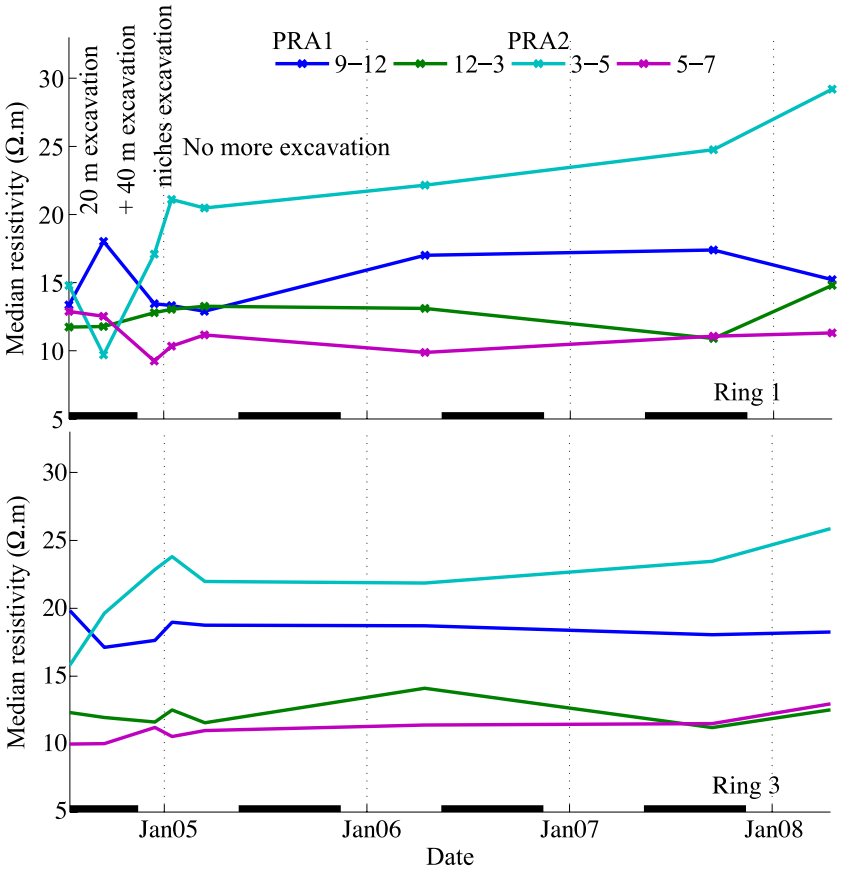

Figure 11. Evolution of the median resistivity with time in the different sectors surrounding the gallery from the surface to a depth of 1.5 m. Black lines indicate summers as the gallery environment is more humid in summer than in winter. Graphics correspond to rings 1 and 3 from top to bottom. The location of the different sectors are represented Fig. 8 with the corresponding colours.

puzzling and appear largely controlled by the local (i.e. at metric scale along the gallery) response to stress perturbation.

4.4.2 Long timescale

Between 2005 March and 1 yr later in 2006 April we observe on ring 1 an increase in resistivity in sectors 9hr–12hr and 3hr–5hr that may be due to the continuation of buckling formation. By the contrary, regions not concerned by EDZ present a slight decrease (Fig. 11). On ring 3 however, variations are much more attenuated, except on the 12hr–3hr sector as its lower part shows an increase of resistivity.

Due to the lack of a regular data sampling and of independent temporal data, it is difficult to interpret resistivity variations over a long timescale. Seasonal variations on temperature and humidity may have an effect on the electrical resistivity in the superficial regions as discussed in Section 2. The closing of joints related to the increase of humidity in summer would induce a decrease of the rock mass resistivity, while the reopening of joints as the superficial rock layer is subject to discharge during the winter season would generate an increase in resistivity (Möri *et al.* 2010). Regions concerned by EDZ could also present a progression of damage by buckling, whereas the clay sealing properties could progressively reduce growth of damaged regions (Meier *et al.* 2000; Blümling *et al.* 2007). However, further studies would be necessary to distinguish the progression or the sealing of the EDZ with effects due to environmental variations. Measurements on a longer time period with a monthly rate should then be replicated to confirm the rock behaviour and its impact on the electrical measurements.

4.5 Importance of anisotropy

The fabric and the bedding of Opalinus Clay generate anisotropy in its physical properties, such as seismic velocities and electrical resistivity (Nicollin *et al.* 2008, 2010; Thovert *et al.* 2011). For instance, *P*-wave velocity equals $2490 \pm 45\,\mathrm{m\,s^{-1}}$ in the direction normal to the bedding and $3330 \pm 90\,\mathrm{m\,s^{-1}}$ parallel to the bedding (Nicollin *et al.* 2008). Electrical resistivity is even more anisotropic and Nicollin *et al.* (2010) found values of $8.5 \pm 2\,\Omega\,\mathrm{m}$ parallel to bedding and of $74 \pm 15\,\Omega\,\mathrm{m}$ and even $200 \pm 37\,\Omega\,\mathrm{m}$ perpendicular to bedding in the EZG-08 experimental area.

The anisotropy of electrical resistivity is not accounted for in this paper and it will deserve further studies using extended data sets yet to be acquired (see Nicollin *et al.* 2010 for a discussion concerning the data needed to invert anisotropy of resistivity). Therefore, we cannot exclude that some of the resistivity variations observed in the tomograms may be partly due to anisotropic effects. Beside the difficulty to acquire data to study anisotropy, it must be quoted that the inversion of anisotropic resistivity suffers from an essential non-uniqueness and the model constraints necessary to obtain reliable solutions remain an active mathematical issue (Kohn & McKenney 1990; Pain *et al.* 2003; Herwanger *et al.* 2004; Adler & Lionheart 2011).

5 CONCLUSIONS

The ERT experiments discussed in this study in light of our up-to-date understanding of the EDZ formation in the Opalinus Clay of the Mont Terri laboratory gives further insights on the technique. Electrical measurements are indeed sensitive to the presence of EDZ and high contrast of electrical resistivity are observed with values ranging in the interval [5–100] Ω m on the reconstructed tomograms corresponding to each electrodes ring set-up. Rings of electrodes separated by only 1 m show significantly differing resistivity structures reflecting the strong variability of the EDZ along the gallery axis. As data coverage is poor inducing 2-D reconstructions and as the anisotropy is not yet taken into account in the model only qualitative information could be extracted from the resulting images.

The reconstructed electrical resistivity images performed to monitor the Mont Terri gallery 04 during the process of its excavation shows a spatial variation correlated with geological and structural features. The images provide then indication on the resistivity values in regions concerned or not by EDZ. The electrical resistivity of undisturbed zone varies between 10 and 13 Ω m, while the resistivity of the EDZ varies between 15 and 100 Ω m depending on the degree of fracturing. Important resistivity variations are observed at distances of about 1 m along the gallery highlighting the damage dependence on local conditions. Short-time variations of resistivity occur within the 6 months following the excavation in response to EDZ creation and equilibration. These short-time variations appear puzzling and complex due to the influence of local conditions. Long time variations of resistivity show an evolution of the EDZ during at least the 3 yr covered by the data. Further measurements regularly spaced and independent data would be required to distinguish the evolution of the EDZ from the influence of temperature and humidity seasonal variations.

ACKNOWLEDGEMENTS

This work benefitted from invaluable help from the whole staff of the FORPRO research programme. We are very thankful to Dale Rucker and an anonymous reviewer for their instructive comments that helped us to improve the manuscript. This work is financially supported by the Centre National de la Recherche Scientifique (CNRS) and Agence Nationale pour la gestion des Déchets RAdioactifs (ANDRA) through MO-A (long term and multi-scale monitoring with passive geophysical methods) project of the FORPRO II programme. Financial support of the experimental work at Mont Terri was provided by the NF-PRO European programme and additional funding from NSERC (Natural Sciences and Engineering Research Council) Canada. Detailed information concerning the Mont Terri URL may be found at www.mont-terri.ch. This is IPGP (Institut de Physique du Globe de Paris) contribution 3414.

REFERENCES

Adler, A. & Lionheart, W.R.B., 2006. Uses and abuses of EIDORS: an extensible software base for EIT, *Physiol. Meas.,* **27,** S25–S42.

Adler, A. & Lionheart, W.R., 2011. Minimizing EIT image artefacts from mesh variability in finite element models, *Physiol. Meas.,* **32,** 823–834.

Alheid, H.J., Kruschwitz, S., Schuster, K. & Yaramanci, U., 2002. Charakterisierung der Auflockerungszone um Strecken im Opalinuston mit seismischen und geoelektrischen Verfahren, *Z. Angew. Geol.,* **48,** 48–55.

Blümling, P., Bernier, F., Lebon, P. & Derek Martin, C., 2007. The excavation damaged zone in clay formations time-dependent behaviour and influence on performance assessment, *Phys. Chem. Earth,* **32,** 588–599.

Bossart, P., Trick, T., Meier, P.M. & Mayor, J.C., 2004. Structural and hydrogeological characterisation of the excavation-disturbed zone in the Opalinus Clay (Mont Terri Project, Switzerland), *Appl. Clay Sci.,* **26,** 429–448.

Cheng, K.S., Isaacson, D., Newell, J.C. & Gisser, D.G., 1989. Electrode models for electric current computed tomography, *Biomed. Eng.,* **36,** 918–924.

Ellis, R.G. & Oldenburg, D.W., 1994. The pole-pole 3-D DC-resistivity inverse problem: a conjugate gradient approach, *Geophys. J. Int.,* **119,** 187–194.

Fletcher, R. & Reeves, C.M., 1964. Function minimization by conjugate gradients, *Comput. J.,* **7,** 149–154.

Friedel, S., 2003. Resolution, stability and efficiency of resistivity tomography estimated from a generalized inverse approach, *Geophys. J. Int.,* **153,** 305–316.

Gibert, D., Nicollin, F., Kergosien, B., Bossart, P., Nussbaum, C., Grislin-Mouëzy, A., Conil, F. & Hoteit, N., 2006. Electrical tomography monitoring of the excavation damaged zone of the Gallery 04 in the Mont Terri rock laboratory: field experiments, modelling, and relationship with structural geology, *Appl. Clay Sci.,* **33,** 21–34.

Günther, T., Rücker, C. & Spitzer, K., 2006. Three-dimensional modelling and inversion of DC resistivity data incorporating topography—II. Inversion, *Geophys. J. Int.,* **166,** 506–517.

Hayley, K., Bentley, L.R., Gharibi, M. & Nightingale, M., 2007. Low temperature dependence of electrical resistivity: implications for near surface geophysical monitoring, *Geophys. Res. Lett.,* **34,** L18402, 1–5.

Hayley, K., Bentley, L.R. & Pidlisecky, A., 2010. Compensating for temperature variations in time-lapse electrical resistivity difference imaging, *Geophysics,* **75**(4), WA51–WA59.

Herwanger, J.V., Pain, C.C., Binley, A., De Oliveira, C.R.E. & Worthington, M.H., 2004. Anisotropic resistivity tomography, *Geophys. J. Int.,* **158,** 409–425.

Kohn, R.V. & McKenney, A., 1990. Numerical implementation of a variational method for electrical impedance tomography, *Inverse Probl.,* **6,** 389–414.

Kruschwitz, S. & Yaramanci, U., 2004. Detection and characterization of the disturbed rock zone in claystone with the complex resistivity method, *J. appl. Geophys.,* **57,** 63–79.

Le Gonidec, Y. *et al.*, 2012. Field-scale acoustic investigation of a damaged anisotropic shale at the Mont Terri Underground Rock Laboratory, Switzerland: effect of a gallery excavation, *Int. J. Rock. Mech.,* **51,** 136–148.

Maineult, A. *et al.*, 2013. Anomalies of noble gases and self-potential associated with geology and fluid dynamics in a horizontal borehole, Mont Terri Underground Rock Laboratory, *Eng. Geol.,* **156,** 46–57.

Marescot, L., Palma Lopes, S., Rigobert, S. & Green, A.G., 2008. Nonlinear inversion of geoelectric data acquired across 3D objects using a finite-element approach, *Geophysics,* **73,** 121–133.

Marschall, P., Distinguin, M., Shao, H., Bossart, P., Enachescu, C. & Trick, T., 2006. Creation and evolution of damage zones around a microtunnel in a claystone formation of the Swiss Jura mountains. SPE Paper 98537.

Mayor, J.C., Velasco, M. & Garcia-Sineriz, J.L., 2007. Ventilation experiment in the Mont Terri underground laboratory, *Phys. Chem. Earth,* **32,** 616–628.

Meier, P., Trick, T., Blümling, P. & Volckaert, G., 2000. Self-healing of fractures within the EDZ at the Mont Terri Rock Laboratory: results after one year of experimental work, in *Proceedings of International Workshop on Geomechanics, Hydromechanical and Thermohydro-mechanical Behaviour of Deep Argillaceous Rocks: Theory and Experiment,* pp. 267–274, eds Hoteit, N., Su, K., Tijani, M. & Shao, J.F., Swets & Zeitlinger.

Möri, A., Bossart, P., Matray, J.M., Frank, E., Fatmi, H. & Ababou, R., 2010. Mont Terri Project cyclic deformations in the Opalinus Clay, in *Proceedings of the Meeting 'Nantes 2010',* ANDRA.

Nicollin, F., Gibert, D., Bossart, P., Nussbaum, C. & Guervilly, C., 2008. Seismic tomography of the excavation damaged zone of the Gallery 04 in the Mont Terri Rock Laboratory, *Geophys. J. Int.,* **172,** 226–239.

Nicollin, F., Gibert, D., Lesparre, N. & Nussbaum, C., 2010. Anisotropy of electrical conductivity of the excavation damaged zone in the Mont Terri Underground Rock Laboratory, *Geophys. J. Int.,* **181,** 303–320.

Nussbaum, C., Bossart, P., Amann, F. & Aubourg, C., 2011. Analysis of tectonic structures and excavation induced fractures in the Opalinus Clay, Mont Terri underground rock laboratory (Switzerland) *Swiss J. Geosci.,* **104,** 187–210.

Pain, C.C., Herwanger, J.V., Saunders, J.H., Worthington, M.H. & de Oliveira, C.R., 2003. Anisotropic resistivity inversion, *Inverse Probl.,* **19,** 1081–1112.

Pessel, M. & Gibert, D., 2003. Multiscale electrical impedance tomography, *J. geophys. Res.,* **108,** 2054 (1–12).

Polydorides, N. & Lionheart, W.R.B., 2002. A Matlab toolkit for three-dimensional electrical impedance tomography: a contribution to the Electrical Impedance and Diffuse Optical Reconstruction Software project, *Meas. Sci. Technol.,* **13,** 1871–1883.

Rücker, C., Günther, T. & Spitzer, K., 2006. Three-dimensional modelling and inversion of DC resistivity data incorporating topography—I. Modelling, *Geophys. J. Int.,* **166,** 495–505.

Schöberl, J., 1997. NETGEN—an advancing front 2D/3D-mesh generator based on abstract rules, *Comput. Vis. Sci.,* **1,** 41–52.

Schuster, K., Alheid, H.J. & Boddener, D., 2001. Seismic investigation of the excavation damaged zone in Opalinus Clay, *Eng. Geol.,* **61,** 189–197.

Thovert, J.F., Mourzenko, V.V., Adler, P.M., Nussbaum, C. & Pinettes, P., 2011. Faults and fractures in the Gallery 04 of the Mont Terri rock laboratory: characterization, simulation and application, *Eng. Geol.,* **117,** 39–51.

Wassermann, J., Sabroux, J.C., Pontreau, S., Bondiguel, S., Guillon, S., Richon, P. & Pili, E., 2011. Characterization and monitoring of the excavation damaged zone in fractured gneisses of the Roselend tunnel, French Alps, *Tectonophysics,* **503,** 155–164.

Yong, S., Kaiser, P.K. & Loew, S., 2010. Influence of tectonic shears on tunnel-induced fracturing, *Int. J. Rock Mech. Min. Sci.,* **47,** 894–907.

APPENDIX A: RECONSTRUCTION OF THE RESISTIVITY DISTRIBUTION

For our numerical modelling, we chose the finite element (FE) method to reproduce the actual shape of the gallery. The FE model was used to compute the apparent resistivity corresponding to a given resistivity distribution. It constituted the forward model, f, embedded in an inverse problem that aimed at calculating a resistivity distribution capable of reproducing a facsimile of the measured data. The parametrization of the inverse problem, that is, the manner by which the resistivity distribution was represented, was chosen to account for the geometry of the acquisition system.

A1 FE forward modelling

An FE model represents the medium surrounding the gallery and may include or not its end-face or the HG-A and EZ-B niches. For given conductivities allocated to the model elements, the forward problem computes the apparent resistivities to be compared with the measured ones.

A1.1 Geometrical model of the gallery

The cross-section of the tunnel was approximated by an ellipse and a slightly tilted ground fitted to the positions of the electrodes of the three rings. This cross-section was extruded along the gallery axis over a length of 64 m with the NETGEN software (Schöberl 1997) to obtain the 3-D model (Fig. A1). The nodes of the mesh elements were moved to correspond to the electrodes position of each ring, as the electrode positions varied slightly from one ring to another. The external boundary of the model was a cylinder with a radius of 30 m and was sufficiently large to avoid boundary effects.

The size of the mesh elements increased as a function of distance from the electrodes to account for sensitivity of the resistivity method (Rücker *et al.* 2006). The complete electrode model implemented in EIDORS (Cheng *et al.* 1989) was used with an electrode

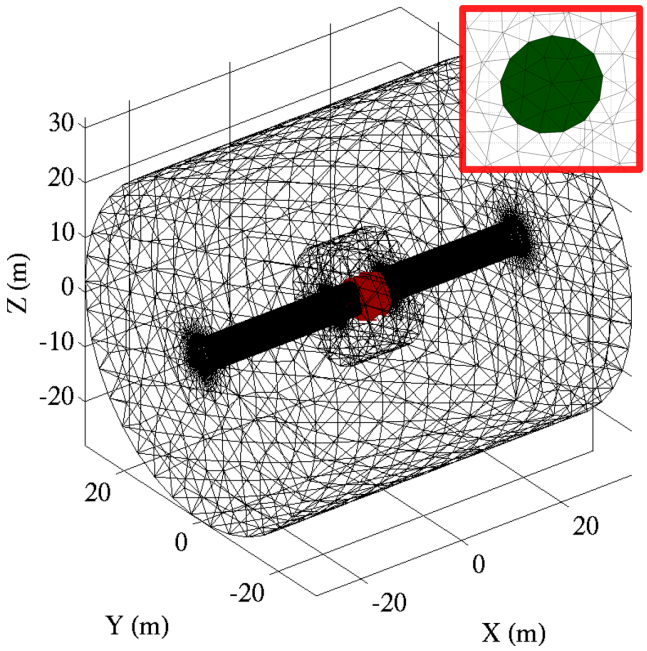

Figure A1. Finite element model of the rock mass surrounding the studied gallery. The mesh is defined coarser away from the electrodes located in the red area. In the red square, an illustration of one electrode circular model.

contact impedance of 0.01 Ω to represent the high conductivity of steel.

Different FE models were constructed to account for the successive excavation stages of the gallery and gallery niches. The FE model of Fig. A1 was used to analyse data acquired in 2004 September and December and was modified to produce two complementary models: one with the end-face nearby the rings and representing the situation in 2004 July and the other one with the EZ-B and HG-A niches, valid after 2005 January. An outer shotcrete layer applied to the gallery wall had a thickness that varied between 10 and 30 cm, with a resistivity (650 Ω m), that was much larger than the resistivity ($6 < \rho < 60\,\Omega$ m) of Opalinus Clay (Kruschwitz & Yaramanci 2004; Gibert *et al.* 2006; Mayor *et al.* 2007). Consequently, the shotcrete layer is not included in the FE model.

A1.2 Forward solution

The forward model f computes the N synthetic voltages $\tilde{\mathbf{V}} = (\tilde{V}_1, \tilde{V}_2, ..., \tilde{V}_N)^t$ for a given conductivity distribution $\boldsymbol{\sigma} = (\sigma_1, \sigma_2, ..., \sigma_M)^t$,

$$\tilde{\mathbf{V}} = f(\boldsymbol{\sigma}). \tag{A1}$$

The voltages are then converted into apparent resistivities $\tilde{\boldsymbol{\varrho}}$ by using the N geometrical factors $\boldsymbol{\phi}$:

$$\tilde{\varrho}_n = \phi_n \tilde{V}_n / I_n \quad \text{for } n = 1, \ldots, N, \tag{A2}$$

where I_n is the injected current. For a medium with a constant resistivity ρ_0, the geometrical factor ϕ_n is such that $\tilde{\varrho}_n = \rho_0$. The apparent resistivity depends then on the resistivity distribution in the medium and no more from the geometry of the acquisition system or from the medium topography (Gibert *et al.* 2006). In practice, the forward problem is solved with the EIDORS functions (Polydorides & Lionheart 2002; Adler & Lionheart 2006) with insulating boundary conditions on both the gallery walls and all outer boundaries of the model, except at the current electrodes where a Neumann condition is imposed to represent an electrical current of 100 mA.

A2 Inverse problem

The objective of the inverse problem is to recover the resistivity distributions capable of reproducing the measured apparent resistivity $\boldsymbol{\varrho} = (\varrho_1, \varrho_2, ..., \varrho_N)^t$. Due to the huge number $M \approx 5 \times 10^5$ of elements constituting the FE model, directly retrieving $\boldsymbol{\sigma} = (\sigma_1, \sigma_2, ..., \sigma_M)^t$ from a moderate number of data (say 500 to 1000) constitutes an underdetermined problem that necessitates a reduction in the number of degrees of freedom.

We explicitly defined the unknown conductivities $\tilde{\boldsymbol{\sigma}} = (\tilde{\sigma}_1, \tilde{\sigma}_2, ..., \tilde{\sigma}_K)^t$ on a coarse mesh with K elements and use $\tilde{\boldsymbol{\sigma}}$ to interpolate the $\boldsymbol{\sigma}$ in the finely meshed forward FE model (Pessel & Gibert 2003; Günther *et al.* 2006; Rücker *et al.* 2006). By this way, we have $K \approx N \ll M$ while keeping a direct control on the parametrization of the unknown conductivity $\tilde{\boldsymbol{\sigma}}$. A $M \times K$ matrix $\mathbf{M}$ is constructed to establish a correspondence between the $\tilde{\sigma}_k$ and the σ_m: $\boldsymbol{\sigma} = \mathbf{M}\tilde{\boldsymbol{\sigma}}$. Following this approach, each plane containing the rings uses a coarse 2-D mesh and the $\tilde{\sigma}_k$ are assigned to the elements of this 2-D grid (Fig. 8). We use linear interpolation for σ_m in and between the rings' planes and we extrude σ_m from rings 1 and 3 to the edges of the model.

Concentric homothetic layers make up the three coarse 2-D grids, each having the shape of the gallery for a depth of 6 m. The first layer has a thickness of 10 cm, the next ones have a thickness of 20 cm out to 4 m, and last layers have a thickness of 50 cm. Angular sectors divide the layers as shown in Fig. 8. For this coarse meshing, the number of unknown conductivities $\tilde{\sigma}_k$ is $K = 334 \times 3 = 1032$.

Beyond a depth of 6 m, the model resistivity remains constant with a value of 11 Ω m as determined from the borehole data sets, described in the Appendix B. We assume that no damage were produced by the gallery excavation at such depth and that other processes due to the gallery environment variations, such as temperature or humidity fluctuations do not have any effect neither at a such depth. The starting homogeneous model in the iterative inversion procedure also uses the background resistivity value of 11 Ω m.

The inverse model is constrained by a log-transformed quantity of the conductivities, $\varsigma_k = -\ln(\sigma_k)$, to make the parametrization equivalent for either the conductivity or the resistivity (Friedel 2003; Pessel & Gibert 2003; Günther *et al.* 2006; Marescot *et al.* 2008; Nicollin *et al.* 2010). The inversion is performed with an iterative conjugate gradient method regularized through an analysis of the Jacobian singular values (Fletcher & Reeves 1964; Ellis & Oldenburg 1994; Günther *et al.* 2006; Marescot *et al.* 2008). The residuals obtained for each data set are summarized in Table A1.

Table A1. Median of the residuals for all data sets.

Acquisition	Ring 1 (per cent)	Ring 2 (per cent)	Ring 3 (per cent)
2004 July	7.1	11.1	7.1
2004 September	4.6	5.9	4.6
2004 December	4.7	6.0	4.8
2005 January	4.5	5.8	4.8
2005 March	4.8	5.4	4.5
2006 April	4.8	5.9	4.4
2007 September	4.6	7.4	4.1
2008 April	5.1	6.4	6.2
Average	5.0	6.7	5.1

APPENDIX B: DETERMINATION OF THE BACKGROUND RESISTIVITY

To determine the background resistivity, data sets acquired in boreholes located close to the electrodes' rings were analysed using the same process as the data acquired on rings. The data quality was studied using reciprocal measurements and data showing a difference higher than 25 per cent were rejected. The measured voltages were converted into apparent resistivity as for the rings' data sets.

B1 Boreholes data sets

Three boreholes, BEZ-G1, G2 and G4 were drilled on the gallery floor with a diameter of 131 mm and a depth of 7 m, between the electrode rings 2 and 3 (see Fig. 3).

32 electrodes made by lead sheets were placed on a 6-m long wood strip with a step of 15 cm. The coupling of the electrodes with the medium was insured by an inflatable pipe pressing the electrodes against the rock as in the experiment developed by Maineult *et al.* (2012). The first electrode was located at a depth of 1.05 m, allowing the medium to be sounded to a depth of 5.7 m. Data were acquired in four cardinal directions with a Wenner configuration and its reciprocal.

B2 Estimation of the undisturbed area resistivity

An inversion is computed to estimate the resistivity at a depth higher than 3 m, assuming an axial symmetry around each borehole. As for rings' data sets, an FE model is constructed to represent the resistivity surrounding the boreholes. The model presents a cylinder shape with a diameter and a length of 30 m, the borehole is included with a diameter of 13 cm and a depth of 7 m. The shape of the rectangular electrodes with a dimension of $4 \times 2\,\mathrm{cm}^2$ is taken into account.

A coarser mesh is then constructed to reduce the number of sought values, assuming an axial symmetry around each borehole. It is restricted to a depth of 7 m and a radial distance of 2 m from the borehole wall. The inversion is computed with the conjugate gradient method described in the paper in five iterations. The homogeneous value of the initial model is first estimated by a linear fitting of the data sets. The median value of the resistivities reconstructed at a depth higher than 3 m and at a radial distance higher than 15 cm is computed to estimate the background resistivity. This median value equals 10.55, 10.83 and 11.83 Ω m, for BEZ-G1, G2 and G4, respectively. So a resistivity value of 11 Ω m is allocated to the background during the inversion of the rings' data sets.